ARPES on $Na_{0.6}CoO_2$: Fermi Surface and Unusual Band Dispersion

H.-B. Yang,[1] S.-C. Wang,[1] A. K. P. Sekharan,[1] H. Matsui,[2] S. Souma,[2] T. Sato,[2] T. Takahashi,[2] T. Takeuchi,[3] J. C. Campuzano,[4] R. Jin,[5] B. C. Sales,[5] D. Mandrus,[5] Z. Wang,[1] and H. Ding[1]

[1]*Department of Physics, Boston College, Chestnut Hill, Massachusetts 02467, USA*
[2]*Department of Physics, Tohoku University, 980-8578 Sendi, Japan*
[3]*Research Center for Advanced Waste and Emission Management, Nagoya University, Japan*
[4]*Department of Physics, University of Illinois at Chicago, Chicago, Illinois 60607, USA*
[5]*Condensed Matter Science Division, Oak Ridge National Laboratory, Oak Ridge, Tennessee 37831, USA*

(Received 22 October 2003; published 18 June 2004)

The electronic structure of single crystals $Na_{0.6}CoO_2$, which are closely related to the superconducting $Na_{0.3}CoO_2 \cdot yH_2O$ ($T_c \sim 5$ K), is studied by angle-resolved photoelectron spectroscopy. While the measured Fermi surface (FS) is consistent with the large FS enclosing the Γ point from the band theory, the predicted small FS pockets near the K points are absent. In addition, the band dispersion is found to be highly renormalized, and anisotropic along the two principal axes (Γ-K, Γ-M). Our measurements also indicate that an extended flatband is formed slightly above E_F along Γ-K.

DOI: 10.1103/PhysRevLett.92.246403 PACS numbers: 71.27.+a, 71.18.+y, 74.25.Jb, 74.70.–b

The recent discovery of superconductivity in $Na_xCoO_2 \cdot yH_2O$ ($T_c \sim 5$ K) [1] has generated great interest in the condensed matter physics community. Over the past 17 yr, the study of high-T_c superconductivity has focused on copper oxide compounds (cuprates). The unexpected finding of superconductivity in cobalt oxide (cobaltates) raises the hope that it may help solve the high-T_c problem. Similar to the cuprates, Na_xCoO_2 has a layered structure. However, unlike the cuprates that have a square lattice in the plane, the cobaltate has a hexagonal lattice. Electronically, both compounds have partially filled $3d$ orbitals. In the cuprates, the Cu^{2+} has a $3d^9$ configuration, and forms the highest e_g ($d_{x^2-y^2}$) band near E_F, which hybridizes with the O $2p$ orbital. In the cobaltates, the electronic configuration of Co^{4+} is $3d^5$, which occupies three lower t_{2g} bands, with the topmost being $A_{1g} = (d_{xy} + d_{yz} + d_{zx})/\sqrt{3}$. The hybridization with the O $2p$ orbital is greatly reduced due to the weaker overlap of the triangular bonding and the fact that the relevant orbitals in the cobaltates are t_{2g} rather than e_g as in the cuprates.

In addition to these similarities, another important connection between the two materials is that both of them have strong electron correlations. It is widely believed that the physics of the high-T_c cuprates is that of a doped Mott insulator. The cobaltate can also be regarded as an electron-doped Mott insulator. The spin configuration in the frustrated half-filled triangular lattice may favor a resonating-valence bond (RVB) state [2], and superconductivity in the vicinity of such the RVB state may prefer a d-wave order parameter [3], similar to the cuprates. Moreover, the superconducting phase diagram of $Na_xCoO_2 \cdot 1.3H_2O$ is found to have a dome shape [4], similar to the cuprates.

There also exist similarities between Na_xCoO_2 and another layered oxide superconductor Sr_2RuO_4 (ruthenate), which is believed to be a p-wave superconductor. The two materials have similar behaviors in transport and magnetic susceptibility [5,6]. In addition, both materials exhibit ferromagnetic fluctuations at low temperatures [7,8], which are believed to be responsible for the p-wave pairing in the ruthenate. Indeed a p-wave triplet superconducting state has been suggested for the cobaltate [9]. In addition, we note that both materials have the same electron filling level ($\frac{3}{4}$) for the maximum superconductivity. This is further away from half-filling than in the cuprates, where the filling number of 1 ± 0.16 is usually regarded as the optimal doping level.

Band structure and Fermi surface (FS) topology are known to be important in understanding unconventional superconductivity. Different electronic structures may induce different fluctuation, which can lead to different pairing symmetry. In this Letter, we report an angle-resolved photoelectron spectroscopy (ARPES) study on $Na_{0.6}CoO_2$ single crystals. Although $Na_{0.6}CoO_2$ is not a superconductor, a reduction of the Na concentration and proper hydration can turn this material into a superconductor [1]. It is worth mentioning that $Na_{0.5}CoO_2$ has a large thermoelectric power ($S \sim 100$ mV/K at 300 K), which is 1 order of magnitude larger than in typical metals and high-T_c cuprates [5]. In our ARPES study, we observe clear band dispersion and FS crossings in $Na_{0.6}CoO_2$. While the observed FS location agrees with the large FS predicted by local-density approximation (LDA) band theory [10], the predicted small FS pockets near the K points are not observed. The observed Fermi velocity for the near-E_F band is renormalized and anisotropic along the two principal axes (Γ-M, Γ-K). The Fermi velocity is reduced by a factor of 3 along Γ-M, and 5–10 along Γ-K. In addition, we observe an unusual band splitting along Γ-M, which is however absent along Γ-K.

High-quality Na_xCoO_2 single crystals are grown using the floating-zone method. The Na composition $x \approx 0.6$ is determined by inductively coupled plasma atomic emission spectroscopy [11]. ARPES experiments are performed at the Synchrotron Radiation Center, Wisconsin. The energy resolution is ~10–20 meV, and the momentum resolution ~0.02 $Å^{-1}$. Samples are cleaved and measured *in situ* in a vacuum better than 8×10^{-11} Torr at low temperatures (20–40 K) with a flat (001) surface. The sample is stable and shows no sign of degradation during a typical measurement period of 12 h. The sample is oriented according to its Laue diffraction pattern.

In ARPES, a sign for a good surface is a clear valence band dispersion, which is observed in this material, as shown in Fig. 1. We measure the valence band at a number of photon energies, ranging from 16–110 eV. The band dispersion is clearly visible, as shown in Fig. 1(a), where a set of energy distribution curves (EDCs) along Γ-K are measured with 22 eV photons. In Fig. 1(b), we plot the intensity of the second derivatives of the measured EDCs to display the band dispersion. It can be seen in Fig. 1(b) that the extracted band dispersion has some similarities to the calculated band structure [10]. In Fig. 1(c), we integrate spectra over a large k space to mimic the density of states (DOS) for two different photon energies (22 and 70 eV). Four peaks can be identified at binding energies of 5.9, 4.6, 2.8, and 0.7 eV, respectively, matching well with the band calculation shown in Fig. 1(c) [10]. The band calculation shows that the O $2p$ bands (2 to 7 eV) and the Co $3d$ bands (below 2 eV) are well separated due to a weak Co d-O p hybridization. This is clearly reflected in Fig. 1(c). In addition, a large enhancement of intensity for the 0.7-eV peak with 70-eV photons supports the Co $3d$ characters for this peak, since 70 eV is just above the Co $3p$-$3d$ resonant excitation (~63 eV).

By examining the spectra in the vicinity of E_F, as shown in Fig. 1(d), one can observe a weak but discernible peak sitting on a large "background" which is mainly a tail of the 0.7-eV peak, similar to an earlier ARPES measurement [12]. According to the band calculation, this peak is the Co A_{1g} band which is at the top of the Co t_{2g} manifold and forms a Fermi surface, and the large background is mostly t_{2g} bands. We find, as shown in Fig. 1(d), that the Co $3p$-$3d$ resonant excitation does not necessarily help the enhancement of the A_{1g} peak since the resonance also enhances the background which has the same Co $3d$ character. Experimentally, we find that both 22 and 70 eV photons are suitable in identifying this near-E_F band.

Figure 2 shows dispersing spectra along a principal axis Γ-K, or $(0, 0)$-$(0, \frac{4}{3})$, in the hexagonal reciprocal lattice. The unit of k, used throughout this article, is π/a, where a (2.84 Å) is the nearest Co-Co distance. As seen in Fig. 2(a), a "shoulderlike" peak centered around ~65 meV starts to emerge at $k \sim (0, 0.67)$. With decreasing k_y this peak disperses toward E_F, and seems to cross E_F at ~$(0, 0.5)$. Note that another broad peak around 160–200 meV emerges at $k_y > 0.8$, which has no smooth connection to the A_{1g} band. A careful examination of the spectra indicates that there is a "break" in the dispersion, as shown in Fig. 2(b). Comparing to the calculated band dispersion along Γ-K, this break occurs at almost the same k location where the A_{1g} band intersects with another t_{2g} band, usually called the E_g' band. The E_g' band is predicted to cross E_F and form a small FS pocket near the K point. However, no evidence of this FS crossing is

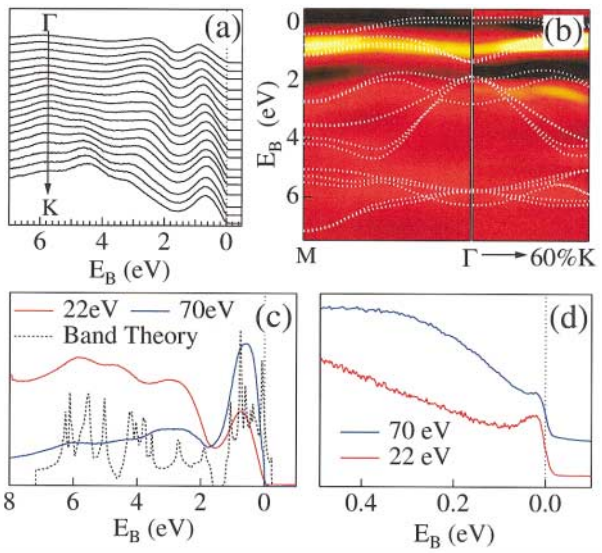

FIG. 1 (color). Valence band of $Na_{0.6}CoO_2$. (a) EDCs along Γ-K ($h\nu = 22$ eV). (b) Intensity plots of second derivatives of spectra along Γ-M and Γ-K. (c) Integrated spectra over a large k space for 22 eV (red) and 70 eV (blue) photons. The dashed line is the total DOS from band theory [10]. (d) Near-E_F EDCs at k_F along Γ-K using 22 eV (red) and 70 eV (blue) photons.

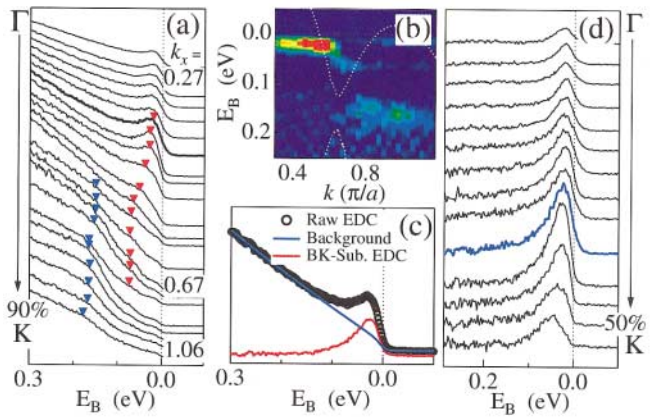

FIG. 2 (color). Near-E_F spectra at 40 K along Γ-K ($h\nu = 22$ eV). (a) EDCs along Γ-K. (b) Intensity plot of second derivatives of the spectra shown in (a). The white dashed lines are from the band calculation [10]. (c) An example of background subtraction. (d) EDCs after background subtraction. The blue curve is at $k_F = (0, 0.5)$.

observed in our experiment, which may result from a shift in the chemical potential due to electron correlations or other many-body interactions. A possible explanation for the break in dispersion is that the electron band interacts with a collective mode. Not that three phonon modes, with an energy of ~55–75 meV, have been observed by a Raman experiment [13].

To see the low-energy excitations more clearly, we subtract the large background from the EDC. One example of the subtraction is demonstrated in Fig. 2(c), where an almost straight line is used for the background. The background-subtracted EDCs along Γ-K are plotted in Fig. 2(d). One can clearly see that an asymmetrical peak disperses toward E_F while its line shape sharpens up. At $k \approx (0, 0.5)$, the peak experiences a substantial reduction in its intensity, indicating that the peak is crossing E_F and the sharp Fermi function removes most of the spectral weight above E_F. After the crossing, a small peak near E_F persists for an extended range of k, from ~(0, 0.5) to (0,0). This indicates that there is an extended flatband just above the E_F. The small peak is the leftover intensity from the Fermi function cutoff. We note that there is an extended flatband in both the cuprates (i.e., $Bi_2Sr_2CaCu_2O_8$) and the ruthenate Sr_2RuO_4. While the influence of the flatband to superconductivity is still under debate, the enhanced DOS near E_F would certainly enhance spin and charge fluctuations, which are found to be strong in all three materials.

ARPES spectra along another principal axis Γ-M, or $(0, 0)$-$[(2/\sqrt{3}), 0]$, are plotted in Fig. 3. Symmetric dispersion can be observed along a long cut in k over different Brillouin zones (BZs). We observe some differences for spectra between Γ-M and Γ-K. One major difference is that there is a band splitting along Γ-M. This splitting can be easily seen if we zoom in at the band crossing, as shown in Figs. 3(c) to 3(e), where we plot the intensity plot, EDCs, and momentum distribution curves (MDCs) in the vicinity of the band splitting. From these three displays, we observe two nearly parallel bands in the vicinity of k_F with an energy separation of ~60 meV and a momentum separation of $\sim 0.1\pi/a$.

We summarize our ARPES results in Fig. 4. In Fig. 4(a), we plot the FS crossings (FSCs) in the hexagonal BZ. For comparison, the calculated FS [10] of $Na_{0.5}CoO_2$ is also plotted in Fig. 4(a). We have measured many samples with several photon energies; the results are consistent. All the FSCs shown in Fig. 4(a) are extracted directly from measurements, and no symmetry operations have been applied here. Note that the FSCs with the same symbols over different BZs are obtained from the same sample during a short time interval. This eliminates potential problems from sample misalignment and surface contamination, and helps accurately determine the size of the FS. As seen from Fig. 4(a), the size of the measured FS in $Na_{0.6}CoO_2$ is somewhat larger than the calculated one in $Na_{0.5}CoO_2$. We also noted that in a recent ARPES study [14] for a more Na-doped sample ($Na_{0.7}CoO_2$), the observed holelike FS appears larger than the one observed here. The observation of a smaller occupied area with more doped electrons apparently violates the Luttinger theorem. It is possible that some electron carriers become localized at higher Na doping levels,

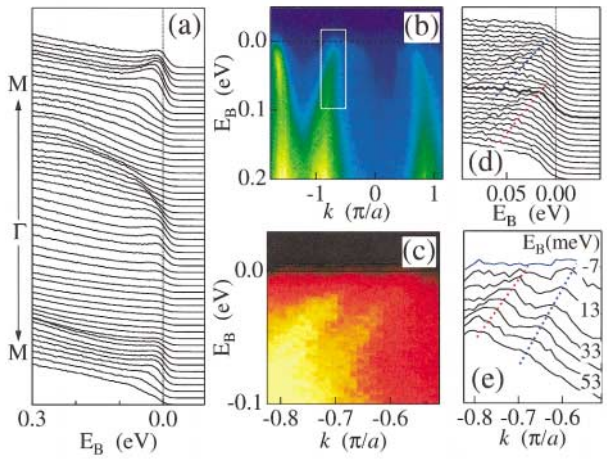

FIG. 3 (color). Near-E_F spectra at 40 K along Γ-M ($h\nu =$ 22 eV). (a) EDCs and (b) E-k intensity plot for a long cut along M-Γ-M. Plots of (c) E-k intensity, (d) EDCs, (e) MDCs magnified from the white box in Fig. 3(b). Dashed lines are the guides for peak positions.

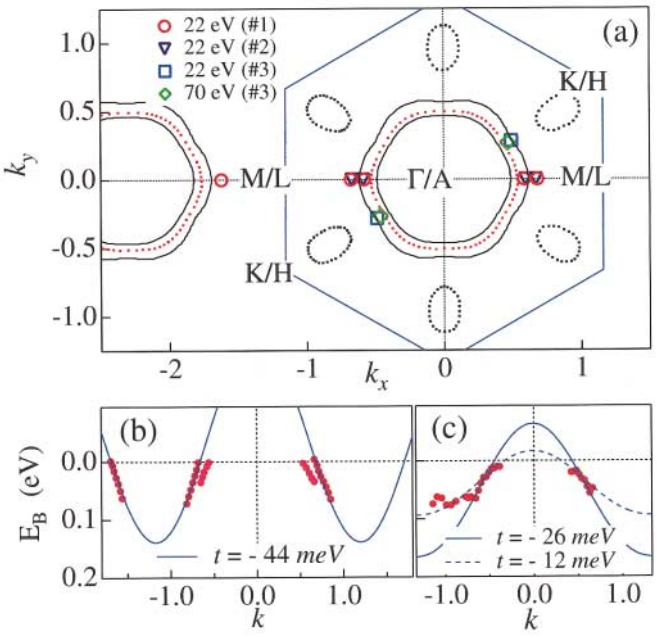

FIG. 4 (color). (a) Measured FS crossings (symbols) compared to calculated FS in $k_z = 0$ (black solid lines) and $k_z =$ 0.5 (red dashed lines) planes. The blue hexagon is the 2D BZ. (b) Extracted band positions along Γ-M (red dots) and a tight binding fit with $t = -44$ meV (solid line). (c) Extracted band positions along Γ-K (red dots) and two tight binding fits with $t = -12$ meV (solid line) and $t = -26$ meV (dashed line).

resulting in a reduction in the number of itinerant electrons that contribute to the area of the FS. This might also explain the unusual ferromagnetic transition observed in highly Na-doped samples [15,16].

We extract the band dispersion from peak positions in MDCs. The extracted band positions along Γ-M and Γ-K are plotted in Figs. 4(b) and 4(c). Reliable values of the dispersion can be obtained from E_F to $\sim$70 meV since beyond this energy the spectral linewidth becomes so broad that its position is ill defined. As seen in Fig. 4(b), the measured band dispersion along Γ-M is nearly linear in the 70-meV range, with a Fermi velocity $v_F \sim 0.41$ eV Å. We use a simple tight binding band on the triangular lattice to fit the measured band dispersion for the outer band:

$$\epsilon_k = -2t\left(\cos k_x + 2\cos\frac{k_x}{2}\cos\frac{\sqrt{3}k_y}{2}\right) - \mu, \qquad (1)$$

where t is the nearest neighbor hopping integral, and μ is the chemical potential. The fitting yields $t \sim 44$ meV (with a negative sign) along Γ-M. The measured dispersion along Γ-K is more complicated, as shown in Fig. 4(c). In addition to the "flat dispersion" around 70 meV due to the break, the dispersion changes its slope at $\sim$20 meV. This slope change may be a consequence of the flatband observed in Fig. 2. While a tight binding fit for the range between E_F and 20 meV yields $t \sim 12$ meV and $v_F \sim 0.12$ eV Å, another fit between 20 and 70 meV produces $t \sim 26$ meV and $v_F \sim 0.24$ eV Å. Both values of t are smaller than the one along Γ-M. The different values of t along the two principal axes are unexpected from a simple tight binding model or LDA band theory. This indicates that either t is k dependent or there may be other factors that modify the band dispersion, such as low-lying modes or energy gaps.

The small value of t, especially along Γ-K ($t \sim$ 12–26 meV), is puzzling, since the superexchange interaction J is also estimated to be small (12–24 meV) in this material [3]. The fact that t and J have the similar values is at odds with the large correlation U. Therefore the small t observed here should be regarded as the effective t_{eff}, which is renormalized from the original band t, estimated to be $\sim$130 meV [the total bandwidth ($12t$) is $\sim$1.6 eV] [10,17]. The reduction of t indicates a strong mass renormalization of a factor of 5–10, which is likely due to the strong correlation in this material. A similar mass renormalization ($\sim$7) is also suggested by a large electronic specific heat coefficient γ (~ 48 mJ/mol K^2) observed in this material [18,19]. We note that both the flat section of the FS and the extended flatband observed along Γ-K would make it the dominant direction in the contribution to the DOS. Therefore, t along Γ-K is more relevant to the specific heat result.

Another surprising finding from this study is a relatively large band splitting along Γ-M. While band theory predicts a bilayer splitting resulting from the two CoO_2 planes per unit cell [10], we cast doubt on this assignment for the following reasons. (i) In the case of the bilayer splitting, the c-axis hopping integral $t_\perp$ would be 30 meV, similar to the in-plane t. This is inconsistent with the large transport anisotropy ($\sigma_{ab}/\sigma_c \sim 200$ at 4 K) [5]. (ii) The two CoO_2 layers in a unit cell have identical geometry for Co atoms, and this would not generate a bilayer splitting for the Co A_{1g} band near E_F which has a very small overlap with oxygen orbitals. In support of this, we note that the band calculation shows no discernible gap at the zone boundary of the doubled unit cell [10]. This suggests that the band can be unfolded to yield a c-axis dispersion rather than a splitting. (iii) No band splitting is observed along Γ-K, which is not consistent with a simple bilayer splitting, although different k_z may modify the size of splitting. It is known that other phenomena, such as itinerant ferromagnetism or surface state, can also cause band and FS splitting. More studies are necessary in order to resolve this issue.

We thank M. Fisher, C. Gundelach, and H. Hochst for technical support in synchrotron experiments, P. D. Johnson, P. A. Lee, N. P. Ong, D. J. Singh, and J. D. Zhang for useful discussions and suggestions. This work is supported by NSF DMR-0072205, DOE DE-FG02-99ER45747, Petroleum Research Fund, and the Sloan Foundation. The Synchrotron Radiation Center is supported by NSF DMR-0084402. Oak Ridge National Laboratory is managed by UT-Battelle, LLC, for the U.S. Department of Energy under Contract No. DE-AC05-00OR22725.

[1] K. Takasa *et al.*, Nature (London) **422**, 53 (2003).
[2] G. Baskaran, Phys. Rev. Lett. **91**, 097003 (2003).
[3] Q. H. Wang, D. H. Lee, and P. A. Lee, Phys. Rev. B **69**, 092504 (2004).
[4] R. E. Schaak *et al.*, Nature (London) **424**, 527 (2003).
[5] I. Terasaki, Y. Sasago, and K. Uchinokura, Phys. Rev. B **56**, R12 685 (1997).
[6] Y. Maeno *et al.*, Nature (London) **372**, 532 (1994).
[7] T. Imai *et al.*, Phys. Rev. Lett. **81**, 3006 (1998).
[8] K. Ishida *et al.*, cond-mat/0308506.
[9] D. J. Singh, Phys. Rev. B **68**, 020503 (2003).
[10] D. J. Singh, Phys. Rev. B **61**, 13 397 (2000).
[11] R. Jin *et al.*, Phys. Rev. Lett. **91**, 217001 (2003).
[12] T. Valla *et al.*, Nature (London) **417**, 627 (2002).
[13] M. N. Iliev *et al.*, Physica (Amsterdam) **402C**, 239 (2004).
[14] M. Z. Hasan *et al.*, preceding Letter, Phys. Rev. Lett. **92**, 246402 (2004).
[15] T. Motohashi *et al.*, Phys. Rev. B **67**, 064406 (2003).
[16] J. L. Gavilano *et al.*, Phys. Rev. Lett. **69**, 100404 (2004).
[17] J. Kuneš, K.-W. Lee, and W. E. Pickett, cond-mat/0308388.
[18] Y. Ando *et al.*, Phys. Rev. B **60**, 10 580 (1999).
[19] F. C. Chou *et al.*, Phys. Rev. Lett. **92**, 157004 (2004).